

Continuum Halos in Nearby Galaxies – an EVLA Survey (CHANG-ES) – I: Introduction to the Survey

Judith Irwin¹, Rainer Beck², R. A. Benjamin³, Ralf-Jürgen Dettmar⁴, Jayanne English⁵,
George Heald⁶, Richard N. Henriksen⁷, Megan Johnson⁸, Marita Krause⁹, Jiang-Tao Li¹⁰,
Arpad Miskolczi¹¹, Silvia Carolina Mora¹², E. J. Murphy¹³, Tom Oosterloo¹⁴,
Troy A. Porter¹⁵, Richard J. Rand¹⁶, D. J. Saikia¹⁷, Philip Schmidt¹⁸,
A. W. Strong¹⁹, Rene Walterbos²⁰, Q. Daniel Wang²¹
and

Theresa Wiegert²²

ABSTRACT

We introduce a new survey to map the radio continuum halos of a sample of 35 edge-on spiral galaxies at 1.5 GHz and 6 GHz in all polarization products. The survey is exploiting the new wide bandwidth capabilities of the Karl G. Jansky Very Large Array (i.e. the Expanded Very Large Array, or EVLA) in a variety of array configurations (B, C, and D) in order to compile the most comprehensive data set yet obtained for the study of radio halo properties. This is the first survey of radio halos to include all polarization products.

In this first paper, we outline the scientific motivation of the survey, the specific science goals, and the expected improvements in noise levels and spatial coverage from the survey. Our goals include investigating the physical conditions and origin of halos, characterizing cosmic ray transport and wind speed, measuring Faraday rotation and mapping the magnetic field, probing the in-disk and extraplanar far-infrared - radio continuum relation, and reconciling non-thermal radio emission with high-energy gamma-ray models. The sample size allows us to search for correlations between radio halos and other properties, including environment, star formation rate, and the presence of AGNs. In a companion paper (Paper II) we outline the data reduction steps and present the first results of the survey for the galaxy, NGC 4631.

Subject headings: ISM: bubbles – (ISM:) cosmic rays – ISM: magnetic fields – galaxies: individual (NGC 4631) – galaxies: magnetic fields – radio continuum: galaxies

¹Dept. of Physics, Engineering Physics & Astronomy, Queen's University, Kingston, ON, Canada, K7L 3N6, irwin@astro.queensu.ca.

²Max-Planck-Institut für Radioastronomie, Auf dem Hügel 69, 53121, Bonn, Germany, rbeck@mpifr-bonn.mpg.de.

³Dept. of Physics, University of Wisconsin at Whitewater, 800 West Main St., Whitewater, WI, USA, 53190, benjamin@wisp.physics.wisc.edu.

⁴Astronomisches Institut, Ruhr-Universität Bochum, 44780 Bochum, Germany, dettmar@astro.rub.de.

⁵Department of Physics and Astronomy, University of Manitoba, Winnipeg, Manitoba, Canada, R3T 2N2,

jayanne_english@umanitoba.ca.

⁶Netherlands Institute for Radio Astronomy (ASTRON), Postbus 2, 7990 AA, Dwingeloo, The Netherlands, heald@astron.nl.

⁷Dept. of Physics, Engineering Physics & Astronomy, Queen's University, Kingston, ON, Canada, K7L 3N6, henriksen@astro.queensu.ca.

⁸National Radio Astronomy Observatory, P. O. Box 2, Greenbank, WV, USA, 24944, mjohnson@nrao.edu.

⁹Max-Planck-Institut für Radioastronomie, Auf dem Hügel 69, 53121, Bonn, Germany, mkrause@mpifr-bonn.mpg.de.

¹⁰Dept. of Astronomy, University of Massachusetts,

1. Introduction

We introduce a new survey to detect radio continuum halos¹ in spiral galaxies using the Karl G. Jansky Very Large Array (hereafter, the Expanded Very Large Array, or EVLA). “Continuum Halos in Nearby Galaxies – an EVLA Survey” (CHANG-ES) is observing 35 nearby edge-on galaxies (Table 1, Fig. 1) in the radio continuum at two frequencies (1.5 GHz and 6 GHz, i.e. in L-band and C-band, respectively) in all polarization products, and over a range of spatial scales. Our overarching goals are to characterize the na-

710 North Pleasant St., Amherst, MA, 01003, USA, jiangtao@astro.umass.edu.

¹¹Astronomisches Institut, Ruhr-Universität Bochum, 44780 Bochum, Germany, miskolczi@astro.rub.de.

¹²Max-Planck-Institut für Radioastronomie, Auf dem Hügel 69, 53121, Bonn, Germany, cmora@mpifr-bonn.mpg.de.

¹³Observatories of the Carnegie Institution for Science, 813 Santa Barbara Street, Pasadena, CA, 91101, USA, emurphy@obs.carnegiescience.edu.

¹⁴Netherlands Institute for Radio Astronomy (ASTRON), Postbus 2, 7990 AA, Dwingeloo, The Netherlands, oosterloo@astron.nl.

¹⁵Hansen Experimental Physics Laboratory, Stanford University, 452 Lomita Mall, Stanford, CA, 94305, USA, tporter@stanford.edu.

¹⁶Dept. of Physics and Astronomy, University of New Mexico, 800 Yale Boulevard, NE, Albuquerque, NM, 87131, USA, rjr@phys.unm.edu.

¹⁷National Centre for Radio Astrophysics, TIFR, Pune University Campus, Post Bag 3, Pune, 411 007, India, djs@ncra.tifr.res.in.

¹⁸Max-Planck-Institut für Radioastronomie, Auf dem Hügel 69, 53121, Bonn, Germany, pschmidt@mpifr-bonn.mpg.de.

¹⁹Max-Planck-Institut für extraterrestrische Physik, Garching bei München, Germany, aws@mpe.mpg.de.

²⁰Dept. of Astronomy, New Mexico State University, PO Box 30001, MSC 4500, Las Cruces, NM 88003, USA, rwalterb@nmsu.edu.

²¹Dept. of Astronomy, University of Massachusetts, 710 North Pleasant St., Amherst, MA, 01003, USA, wqd@astro.umass.edu.

²²Dept. of Physics, Engineering Physics & Astronomy, Queen’s University, Kingston, ON, Canada, K7L 2T3, twiegert@astro.queensu.ca.

¹By ‘halo’, we mean the the gas, dust, cosmic ray, and magnetic field components above a galaxy’s plane, rather than stellar or dark matter halos. We will refer to the region, $0.2 \lesssim z \lesssim 1$ kpc, as the disk-halo interface and use ‘halo’ for emission on larger scales ($z \gtrsim 1$ kpc). ‘High-latitude’ or ‘extraplanar’ are also used to describe either of these components.

ture and prevalence of radio halos, their magnetic fields and the cosmic rays that illuminate those fields. By initiating a survey, we can address the connection between radio halos and the underlying galaxy disk as well as galaxy environment and provide a coherent data set with legacy value for the scientific community.

In this first paper, our goals are to outline the motivation for the survey (Sect. 2), to describe its scientific goals (Sect. 3), to introduce the galaxy sample and its characteristics (Sect. 4), and to detail the EVLA observations, including our specific goals for sensitivity, resolution and spatial coverage (Sect. 5). In a companion paper (Irwin et al. 2012, hereafter, Paper II) we present the first results of the survey from test observations of the galaxy, NGC 4631.

2. Motivation

Since the early pioneering observations of edge-on galaxies (Ekers & Sancisi 1977; Allen, Baldwin & Sancisi 1978; Hummel & van der Hulst 1989; Hummel, Beck, & Dettmar 1991), it has been clear that radio continuum emission can extend well above galaxy disks, that is, to z heights² greater than 500 pc and often to many kpc. Radio continuum emission represents just one component of the multiphase gaseous halos that are typically present. For example, halos have been observed in H α emission and other optical lines (called the ‘extraplanar diffuse ionized gas’ or eDIG), in soft X-ray emission, in the 21 cm HI line, in infra-red (IR) emission from dust, and in molecular species such as CO and PAHs (e.g. Bregman & Houck 1997; Lee et al. 2001; Irwin & Seaquist 1990; Martin & Kern 2001; Heesen et al. 2009a,b; Whaley et al. 2009; Wang et al. 1995, 2001; Howk & Savage 1999; Rossa & Dettmar 2003; Rand 1996). The halo radio continuum emission is primarily from synchrotron radiation (e.g. Irwin, English & Sorathia 1999) implying the presence of cosmic rays (CRs) and magnetic fields out of the plane.

Although radio continuum studies of edge-on galaxies have been conducted in the past (Hummel & van der Hulst 1989; Hummel, Beck, & Dettmar 1991; Dumke et al. 1995; Irwin, English & Sorathia

²The height, z , is measured perpendicular to the plane of a galaxy disk.

1999; Irwin, Saikia, & English 2000), the limited number of galaxies for some of the surveys, frequency coverage, sensitivity limits, and/or ability to detect a variety of spatial scales have made it difficult to systematically and consistently characterize the properties of radio halos. For example, those studies have observed (in the same order as referenced above) 4 galaxies at 1.5 GHz, 181 galaxies at 5 GHz, 6 galaxies at 10.7 GHz, 16 galaxies at 1.4 and 6 GHz, and 16 galaxies at 1.4 GHz. The spatial scales that were detected as well as the sensitivity limits (see below) varied significantly. CHANG-ES is attempting to improve upon previous surveys in a number of ways.

To begin with, a galaxy sample of significant size (Sect. 4) is being observed over a variety of angular spatial scales (Sect. 5). The latter is particularly important since previous observations of sufficient spatial resolution and sensitivity have shown that structure exists in halos on virtually any scale that is observed. The ‘smooth’ halos that are observed on broad scales resolve into discrete features on a variety of smaller scales.

Low frequencies (1.5 and 6 GHz) have been chosen for their sensitivity to non-thermal emission and for the prospects of carrying out Faraday rotation analyses in galaxy disks and halos. Ours will be the first systematic survey for Faraday rotation in galaxy halos. The frequency choice also ensures that complementary data (for example, single dish data) can be obtained, where needed.

CHANG-ES can also now exploit the wide bandwidths that are provided by the EVLA’s Wideband Interferometric Digital ARchitecture (WIDAR) correlator. These wide bandwidths permit unprecedented improvements in continuum sensitivity. For example, the 5 GHz survey of Hummel, Beck, & Dettmar (1991) achieved a best rms noise of $80 \mu\text{Jy beam}^{-1}$ while the 1.4 GHz and 5 GHz surveys of Irwin, English & Sorathia (1999) achieved best rms values of $43 \mu\text{Jy beam}^{-1}$ and $46 \mu\text{Jy beam}^{-1}$, respectively. Our sensitivity limits should improve upon these previous surveys, in some cases by more than an order of magnitude (see Sect. 5).

In addition, the wide bands provide a wealth of spectral information which will be unique to this survey. For example, it is now possible to measure a spectral index *within* a specific observing band (and possibly more than one for strong emission

if there is curvature). We will therefore obtain at least three spectral indices from observations at two frequencies (Sect. 6).

In summary, CHANG-ES improves on previous surveys by observing a large number of galaxies over a variety of well-defined angular spatial scales at two frequencies, and to low noise limits. By exploiting the wide-band capabilities of the EVLA, a wealth of spectral index information is available. Moreover, CHANG-ES is the first survey of edge-on galaxies for which all polarization products will be obtained, providing important information on halo magnetic fields.

3. Science Goals

3.1. Physical Conditions and Origin of Gaseous Halos

The disk-halo interface and broader halo are dynamic entities that connect starkly different environments: the normal ISM of a galaxy disk, and the rarefied intergalactic medium (IGM). A variety of observational evidence (e.g. Dahlem, Lisenfeld, & Golla 1995; Rossa & Dettmar 2003; Strong et al. 2004; Rossa et al. 2008; Tüllman et al. 2006) points to a connection between the supernova rate per unit area in the disk and the intensity of the halo radio continuum, X-ray and eDIG emission. In a few cases, it is also possible to associate discrete disk-halo features with underlying star forming regions, the latter also presumably being a source of eDIG ionization.

Most models have therefore focussed on the critical link between extra-planar gas and star formation-related activity (largely supernovae) in the underlying disk. Such models have included galactic chimneys (Norman & Ikeuchi 1989), fountains (Shapiro & Field 1976), superbubble blowout (Mac Low & Ferrara 1999) and CR-driven Parker instabilities (e.g. Breitschwerdt et al. 1991; Hanasz, Otmianowska-Mazur, & Lesch 2002).

CRs, in particular, appear to be an essential ingredient in driving outflows (e.g. Ipavich 1975; Boulares & Cox 1990; Everett et al. 2008; Everett, Schiller & Zweibel 2010) and it is this component, along with magnetic fields, that are critical to understanding outflow physics. In the disk, for example, CRs, the magnetic field, and hot gas have roughly equal pressures, whereas in the halo far from the plane, the CR and mag-

netic field pressures appear to dominate; however, it is not clear whether such statements are universally true. Although we now have information on the strength and configuration of halo magnetic fields in some galaxies [for reviews, see Krause (2009) and Krause (2011)], an important goal of CHANG-ES is to consistently measure non-thermal pressures in galaxies with a variety of SFRs. Discrete disk-halo features can also be examined for possible associations with star forming sites in the disk.

Yet, in spite of the abundant evidence that links star formation to extra-planar gas, there are still some puzzles that suggest that underlying star formation is not a sufficient explanation for the existence of halos. There is evidence, for example, that a galaxy’s global magnetic field configuration seems not to be influenced by SFR (Krause 2009). Optical line ratios suggest that a source of heating other than photoionization from in-disk sources is required to ionize the eDIG (e.g. Tüllman et al. 2000; Rand et al. 2011); possibilities include shocks, and heating from magnetic reconnection (Zimmer, Lesch, & Birk 1997). In the latter case, for example, specific magnetic field topologies are predicted (Hanasz, Otmianowska-Mazur, & Lesch 2002). In another model (Gissing, Fromang & Dormy 2009) vertical inflow plays a role. In still another, hydraulic jumps at the arm-interarm boundary produce long-lived vertical features (Martos & Cox 1998). SFR also does *not* seem to affect radio continuum scale heights (Krause 2009, 2011).

In addition, evidence for a direct relationship between HI supershells and SFRs is weaker. Expansion energies of some HI supershells, where measurable, appear to be too high to be accounted for assuming reasonable numbers of supernovae and stellar winds (Spekkens, Irwin, & Saikia 2004; Silich et al. 2006, and references therein) and some HI supershells appear to be present outside of the star forming disks of galaxies (Irwin & Seaquist 1990; Chaves & Irwin 2001), prompting suggestions of other sources of energy (but see Chakraborti & Ray (2011)) or that the shells have been formed from impacting external clouds (e.g. Rand & Stone 1996).

The fact that halos *lag* in comparison to the underlying disk (Swaters et al. 1997; Tüllman et al. 2000; Schaap, Sancisi, & Swaters 2000; Lee et al.

2001; Fraternali, Oosterloo, & Sancisi 2004; Heald et al. 2007), and the difficulty in explaining these lags via dynamical/ballistic models with the gas originating in the disk (Fraternali & Binney 2006; Heald et al. 2007) have led to interpretations that include the accretion of external material onto galaxy disks (Oosterloo, Fraternali, & Sancisi 2007; Fraternali et al. 2007). We need to understand the effects of magnetic field pressure and tension on the dynamics of cycling gas (Benjamin 2002) in order to account for energies and velocity gradients in such systems.

It is clear that circulation and/or outflow can have a dramatic effect on the evolution of the galaxy itself, from modifications of the metallicity gradient to understanding the energy and mass budgets of galaxies, to altered SFRs. Mass flux estimates thus far (Bregman & Pildis 1994; Wang et al. 1995; Fraternali et al. 2002) imply that disk-halo outflows are responsible for moving a large amount of gas and may even result in extra-planar star formation (e.g. Tüllman et al. 2003). That a disk-halo flow is responsible for some of the Galactic intermediate-velocity clouds (IVCs) is also likely (e.g. Wakker & van Woerden 1997).

Galactic ‘feedback’ is an important component in Λ CDM numerical models of galaxy formation. Whether feedback is in the form of central starbursts, global starbursts, or active galactic nuclei (AGNs) is not yet known (for a review, see Baugh 2006), but sometimes type Ia supernovae (objects that are normally associated with Population II objects within a galaxy), are implicated as an important driver (Li et al. 2011b; Wang 2010, and references therein). Observations of S0 galaxies and bulges, for example, indicate that observed X-ray halos are weaker than feedback would suggest (e.g. Li et al. 2011b). Moreover some galaxies with *both* weak AGN and star formation can also have soft X-ray luminous halos (e.g. Li et al. 2011a). But the relations of such outflows to the stellar mass and to the galactic environment and evolution history remains uncertain. While radio continuum emission appears to be mainly related to Population I objects as described above, it is important to verify whether this is always true and to search for deviations that may reveal a link to older components.

3.2. Cosmic Ray Transport and Wind Speed

Theoretical and observational effort on the transport mechanism for cosmic rays (diffusive, convective or both) has been carried out for some time (e.g. Strong 1978; Pohl & Schlickeiser 1990; Duric, Irwin, & Bloemen 1998). Cosmic ray electrons (CREs) can lose energy via a variety of processes, i.e. synchrotron, Inverse Compton, adiabatic, ionization, non-thermal Bremsstrahlung, although the latter two can be neglected in normal galaxies (Condon 1992). The relative importance of the remainder depends on environment, but Heesen et al. (2009a) have shown that the shortest timescales are associated with synchrotron and adiabatic losses in the outflow galaxy, NGC 253. An observational consequence (and one that CHANG-ES can look for) is a measurable steepening of the spectral index where adiabatic losses transition to radiative losses (see Sect. 6 for a discussion of the separation of thermal from non-thermal emission). An analysis of the variation of magnetic field strength and radio spectral index with z height, ($B(z)$ and $\alpha(z)$, respectively) can also provide a wealth of information on CR transport.

Outflow velocity is an important datum for input to numerical models of galaxy formation. Since winds are thought to be driven by CRs and couple to the thermal outflow, a measurement of CRE bulk velocity should apply to the thermal wind speed as well. The CRE bulk speed can be determined from the radio scaleheight at several frequencies and the CRE lifetime (Heesen et al. 2009a). Applying this method to more galaxies and in more detail is an important goal of CHANG-ES. The variation of these quantities with position across the disk can also constrain outflow models and provide information on CR transport within the disk as well.

Outflows from galaxies may also be the mechanism whereby the intergalactic medium became magnetized (Kronberg, Lesch, & Hopp 1999). The bulk CRE outflow speed in NGC 253, for example, achieves 300 km s^{-1} in some locations, i.e. greater than the escape velocity, implying that this outflow should enrich the intergalactic medium (Heesen et al. 2009a). Although the conditions in nearby galaxies may differ substantially from

the high redshift universe, we can address very specific issues, such as how outflows scale with SFR, SFR/area, the presence of compact nuclei, and gravitational potential.

3.3. Faraday Rotation and the Origin of Galactic Magnetic Fields

A fundamental question which CHANG-ES may help to address is the origin of the field itself. Seed fields alone should wind up too quickly to account for the polarization angles that are observed in galaxies. The $\alpha - \Omega$ dynamo is thought to be the best alternative for generating observed fields (Beck et al. 1996). Although the mean-field dynamo might operate separately in the disk and halo regimes, the regime with the more active dynamo may ‘enslave’ the other, resulting in a coupling between disk and halo (Moss & Sokoloff 2008; Moss et al. 2010).

Yet in the few cases where halo fields are detected, they can show geometries that are not easily explained by dynamos alone. Indeed, the observational evidence for regular (i.e. dynamo-generated) fields in galaxy halos so far is rather weak – possibly NGC253 (Heesen et al. 2009b) and indirect evidence from polarized intensity asymmetries seen at 20 cm in 7 galaxies (Braun, Heald & Beck 2010). Faraday rotation studies of our own Galaxy also show no coherent vertical field structure at the Sun’s position (Mao et al. 2010).

Rather, the observations appear to support dynamo-generated fields in the disk that couple to outflowing winds (see Krause 2009). For example, in NGC 4631, the field appears to be perpendicular to the disk where star formation is larger, but at larger radii where the SFR declines, the field becomes parallel to the disk again (Krause 2004). ‘X-shaped’ magnetic structures that have been observed in edge-on galaxies have been reproduced by Hanasz, Wóltański, & Kowalik (2009) in global MHD simulations of CR-driven dynamos. In addition, magnetic helicity conservation requires that outflows be present (Shukurov et al. 2006; Sur, Shukurov & Subramanian 2007). The need for winds in explaining magnetic field structures is certainly consistent with the abundant evidence for outflows that has been outlined above.

Understanding the structure of the magnetic

field requires observations of Faraday rotation, which measures the strength of the ordered magnetic field along the line of sight, and synchrotron polarization, which measures the ordered magnetic field in the plane of the sky. Soida et al. (2011) provide an example of the application of rotation measure information to the study of an edge-on galaxy with a radio halo. By utilizing many frequency channels over two frequency bands and obtaining polarization data over a variety of spatial scales, CHANG-ES observations can disentangle these effects and (with models) even start to probe the 3-dimensional structure of the magnetic field. Rotation measure (RM) synthesis techniques described in Brentjens & de Bruyn (2005) and Heald et al. (2009), which make use of the wide frequency response and many channels of the WIDAR correlator, are being employed.

3.4. The FIR-Radio Continuum Correlation

Young hot massive stars become supernovae which are believed to be the main sites of CR acceleration in galaxy disks, and hot massive stars are also important sources of photons that can heat the dust in disks giving rise to FIR emission. This common origin is thought to be at the heart of the FIR-radio continuum relation which has been observed among and within galaxies (e.g. Helou et al. 1985; Murphy et al. 2006).

Since the mean free path of a dust-heating photon is smaller than the diffusion length of a CR electron, a radio image of a galaxy will be a smoothed version of a FIR image. Retrieval of scale length information can provide important information on the star formation timescale and radiation intensity (see Murphy et al. 2008) and on the degree of field ordering (Tabatabaei et al. 2012). Moreover, by separating thermal from non-thermal radio emission (Sect. 6) and correlating the result with IR emission in different wavebands, we can investigate the warm dust-thermal radio correlation and the cold dust-nonthermal radio correlation (e.g. Brar, Irwin & Saikia 2003; Tabatabaei et al. 2007).

In halos far from sites of in-disk SF, one would expect the difference between mean free paths to be greater still, and that the FIR-radio relation may even break down altogether at some scale height. Together with IR images, CHANG-ES

should be able to investigate to what extent the FIR-radio correlation is or is not valid in galaxy halos. Environment may also play an important part. The low density relativistic plasma component of galaxy halos can provide a sensitive tracer to environmental effects. Murphy et al. (2009), for example, have shown that the relation is modified in Virgo Cluster spirals, likely because of galaxy motions with respect to the intra-cluster medium. The CHANG-ES sample includes galaxies within a wide range of environments.

3.5. CRs and High Energy Modeling

Synchrotron emission results from the electron component of CRs and so there is a tight connection between the gamma-ray emission that is produced by CR nuclei and lepton interactions with gas and radiation fields, and the radio continuum emission that CHANG-ES will observe. The GALPROP code³ (Moskalenko & Strong 1998; Moskalenko et al. 2002; Porter et al. 2008; Strong et al. 2000, 2004, 2009, 2010) self-consistently links these and other components in a model of the Galaxy, predicting (polarized and total) broadband fluxes from radio to gamma-ray energies; it also allows for the inference of other parameters such as the escape probability of particles and the diffusion coefficient.

With modifications, this model will be applied to other galaxies to predict synchrotron scale heights together with gamma-ray intensities from each galaxy. Gamma rays give independent information on the energy density of the CRs and hence allow the determination of magnetic field strengths without the assumption of energy equipartition. With the ability to put strict observational limits on galaxy radio halo sizes (one of the largest sources of uncertainty in GALPROP models of the Milky Way) we will be able to constrain the CR diffusion and energy losses for all species (primary/secondary electrons and nuclei). At present, NGC 253 and M82 are the only edge-on galaxies that have been detected in high-energy gamma rays (Acero et al. 2009; Abdo et al. 2010; Acciari et al. 2009), but our gamma-ray flux predictions can be constrained by current upper limits.

X-ray emission generated from inverse-Compton

³<http://galprop.stanford.edu/>

scattering also provides important relevant data. For example, existing X-ray observations from Chandra and XMM-Newton may already be useful for measuring or tightly constraining the hard X-ray (e.g., 2-10 keV) intensity and its spatial distributions in galactic halos. The combination of the X-ray and the radio measurements can be used to measure the magnetic field and CRe density. Future X-ray satellites⁴ may provide additional constraints.

3.6. Disks and Nuclei

Radio continuum emission is a tracer of massive star formation and does not suffer from obscuration as do many other tracers such as H α emission. This is particularly important for galaxies that are edge-on to the line of sight and so have high optical depths at other frequencies. For example, the H α SFR, corrected for obscuration using $\lambda 24 \mu\text{m}$ data (Calzetti et al. 2007) has not been well-calibrated for edge-on galaxies. With corrections for contributions from lower mass stars (e.g. Irwin et al. 2011), the global radio emission in the disks of the CHANG-ES galaxies should therefore provide a good measure of total SFR which can be compared to SFRs from other tracers. The radio spectral index maps can also provide information on locations of star formation and CR transport within the disk (see Sect. 3.2).

Compact radio cores are indicative of the presence of AGNs and we also know that some spiral galaxies exhibit nuclear jets and/or outflows (e.g. Hummel, van Gorkom, & Kotanyi 1983; Wilson & Ulvestad 1983; Irwin & Seaquist 1988). Galaxy bulges are believed to be correlated with central black holes (Gebhardt et al. 2000; Ferrarese & Merritt 2000) but bulgeless systems can also harbour AGNs (Satyapal et al. 2009). Although we have some indication as to whether nuclear activity is present in our galaxy sample (see Table 1, ‘Nuclear Type’), the presence of aligned emission or compact radio cores should help to distinguish whether nuclear activity is present. These results can be compared to information at other wavebands and can also be correlated with galaxy environment.

⁴The Chinese Hard X-ray Modulation Telescope, NASA’s Nuclear Spectroscopic Telescope Array (NuSTAR), and the Indian X-ray satellite, ASTROSAT, are possible examples.

4. The Galaxy Sample

The sample was taken from the Nearby Galaxies Catalog (NBGC, Tully 1988) which lists galaxy parameters in a consistent fashion and also provides other useful data such as a parameter indicating local galaxy density. The criteria for including a galaxy in our sample were:

- a)* Inclination, $i > 75^\circ$, to ensure a nearly edge-on aspect,
- b)* Declinations, $\delta > -23^\circ$, for accessibility (with adequate uv coverage) from the EVLA,
- c)* Blue isophotal diameters, $4 < d_{25}$ (arcmin) < 15 ; the lower limit ensures sufficient spatial resolution and the upper limit avoids large galaxies that would require many pointings and mosaicing.
- d)* Flux densities at 1.4 GHz, $S_{1.4} \geq 23$ mJy, to ensure the likelihood of a detection.

In addition, 3 galaxies which fell just outside of the above limits were also added because they were known to have extraplanar emission and for which good ancillary data were available. These were NGC 5775 ($d_{25} < 4$ arcmin), NGC 4565 ($d_{25} > 15$ arcmin), and NGC 4244 ($d_{25} > 15$ arcmin and $S_{1.4} < 23$ mJy). There are 35 galaxies in total.

Table 1 illustrates the range of properties of the galaxies. The distances range from 3.3 to 42 Mpc, the galaxies’ morphological types span the range of spirals, both barred and unbarred and a variety of nuclear activity types are represented. They are also in a variety of environments (see ρ in Table 1), from apparently isolated galaxies (e.g. NGC 2683) to Virgo Cluster members. A very nice aspect of this survey is that, other than the 3 galaxies mentioned above, we have not specifically targeted galaxies with known halos and, as a result, there are some galaxies in the sample which have not previously been searched for halo emission.

The choice of systems with detectable radio flux suggests that our galaxies are actively forming stars, although contributions from radio cores are also present in some cases. Star formation rates (SFRs, Table 1), however, are modest, the maximum being $20 M_\odot \text{ yr}^{-1}$ (NGC 4666) or, among those with exclusively HII region nuclear spectra (i.e. no known compact nuclear activity) the maximum is $6.4 M_\odot \text{ yr}^{-1}$ (NGC 5792). By comparison, a sample of 417 nearby star forming galaxies (Moustakas & Kennicutt 2006) has SFRs

ranging from 0.03 to approximately $170 M_{\odot} \text{ yr}^{-1}$ (Kennicutt 2008). Thus, our choice of galaxies with radio continuum fluxes above 23 mJy has not imposed a bias to high SFR in our sample. We are probing the halos of ‘normal’ galaxies.

5. EVLA Observations

CHANG-ES has been awarded up to 405 hours of observing time in dynamic scheduling mode at the EVLA. Observations are being carried out at 1.5 GHz and 6 GHz with 500 MHz and 2 GHz bandwidths, respectively⁵. EVLA continuum observations are now made in spectral line mode which facilitates radio frequency interference (RFI) mitigation and also allows for multi-frequency synthesis techniques to be applied during imaging (see Paper II). We are using 2048 spectral channels at 1.5 GHz and 1024 channels at 6 GHz⁶ which also permits the effective application of RM synthesis techniques (Sect. 3.3).

The distribution of time over frequencies and arrays is given in Table 2. These values are best-case estimates, given that the observing time has been awarded in ‘Shared Risk’ mode⁷ during the extensive commissioning period of the EVLA. All polarization products (Stokes I, Q, U, and V) are being obtained.

Observations in the B, C and D array configurations at 1.5 GHz and in C and D configurations at 6 GHz ensure that a variety of spatial scales are probed, as outlined in Sect. 2. Table 2 shows that the linear resolution spans a range from 56 pc to 9.4 kpc, depending on galaxy distance, observing frequency and array configuration. In fact, the new wide bandwidths provide even more flexibility than the table implies since the resolution will vary between the upper and lower ends of each observing band. With appropriate uv weightings, the array can also be ‘tuned’ to a wider range of spatial resolutions.

The *highest* linear resolutions range from 69 pc to 0.88 kpc at 1.5 GHz and 56 pc to 0.71 kpc at

⁵Radio frequency interference may reduce these values somewhat in practice (see Paper II).

⁶Hanning smoothing will effectively set the spectral resolution at twice the channel width.

⁷Time has been granted under the ‘Resident Shared Risk Observing’ (RSRO) program (<https://science.nrao.edu/facilities/evla/early-science/rsro>).

6 GHz, depending on galaxy distance. For science which requires a comparison between galaxies at similar *linear* resolutions, we will either spatially smooth the data, apply appropriate models, and/or limit the number of comparison galaxies, as necessary. An example is a comparison of vertical scale heights between galaxies. A spatial resolution of approximately 500 pc should permit the measurement of a scale height, assuming an exponential decline. At 1.5 GHz, this is possible for all galaxies closer than 24 Mpc (25 out of 35 galaxies) and at 6 GHz, galaxies closer than 30 Mpc (30 out of 35 galaxies) meet this criterion. Note, however, that we may detect emission to much greater distances; for example, the $\lambda 20$ cm map of Hummel & Dettmar (1990) shows the spectacular radio continuum halo of NGC 4631 being traced to at least 10 kpc from the plane.

On the other hand, the largest angular size detectable by the array is fixed by the shortest antenna spacing. At 1.5 GHz, this is 16 arcmin which is comparable to the optical diameter of our largest galaxies (Table 1), but at 6 GHz, the largest detectable angular size is only 4 arcmin. Therefore, missing flux must be supplied by supplementary single-dish observations of the largest galaxies at 1.5 GHz and of all galaxies at 6 GHz⁸. This is especially important in order to derive accurate spectral index maps between 1.5 GHz and 6 GHz and also to derive proper scaleheights at 6 GHz. Details as to how the single dish data will be combined with the EVLA data will be described in a future paper.

At 1.5 GHz, the full width at half maximum of the primary beam (θ_{PB}) is 30 arcmin so only one pointing is necessary for all galaxies. At 6 GHz, however, $\theta_{PB} = 7.5$ arcmin. Considering the sensitivity of the array to emission outside of the primary beam as well as observing time requirements, we have opted to observe all galaxies with $d_{25} > 1.3 \theta_{PB}$ with two pointings. These pointings are placed on the major axis on either side of the nucleus, separated by one-half of the primary beam.

The noise limits (Table 2) improve over previous observations at comparable spatial resolution.

⁸At the time of writing, we anticipate that these data may come from the Greenbank Telescope, which will have wide bandwidth receivers installed in 2012.

Note that the estimated confusion limit applies to the total intensity image and will be lower for Q and U images. In addition, it should be possible to make corrections for confusion in the low resolution data (e.g. D array) using the high resolution (B array) results.

A description of the data reduction procedures for EVLA data are provided in Paper II.

6. On the Separation of Thermal and Non-thermal Emission

Globally, we know that radio continuum emission in galaxies is dominated by the non-thermal component at our observing frequencies. However, the thermal component is not negligible; for example, thermal contributions are typically 12% and 26% of the total flux at 1.5 GHz and 6 GHz, respectively (Condon 1992). Since the bulk of the global emission is from the galaxy’s disk rather than the halo, these fractions should also be typical of disks. Few measurements of spectral index have so far been made in fainter galaxy halos; however, in NGC 4631, halo emission shows a steeper spectral index than the disk (Hummel & Dettmar 1990), implying that the thermal contribution is weaker and possibly negligible in halos.

The highest linear spatial resolutions for CHANG-ES data (≈ 60 pc, Table 2) are sufficient to resolve larger HII regions in normal galaxies (for example, the largest HII regions in M 31 exceed 100 pc Azimlu, Marciniak, & Barmby 2011). Therefore, the thermal fraction could be significant and, indeed, even dominant in some beams in the disk and possibly the disk-halo interface. In Paper II, for example, we show that the simplest explanation for the spectral curvature that is observed in the disk of NGC 4631 at 1.5 GHz is a contribution from thermal emission; we also show that two star forming complexes have flat spectral indices, consistent with thermal emission.

Wideband EVLA observations (together with single-dish data to fill in missing spacings) contain a wealth of information that can help with the thermal/non-thermal problem. With multi-channel observations in two frequency bands, it is possible to obtain at least 3 spectral index measurements, at least one within each band, and one between the two bands at every point. Since a thermal spectrum is characterized by a

known spectral index ($I_\nu \propto \nu^{-0.1}$) which does not vary with frequency, a measurement of 3 spectral indices may be sufficient to separate thermal from non-thermal emission in the case of a constant non-thermal spectral index, α_{NT} . New algorithms, however, are permitting the measurement of changing spectral indices *within* observing bands (see Paper II for details). For positions with sufficient signal-to-noise, curvature in α_{NT} can be detected. This is particularly important for modelling cosmic ray propagation (e.g. Sect. 3.2).

7. Summary

In this paper, we have introduced a new survey, called CHANG-ES, to observe radio continuum halos in 35 edge-on, normal spiral galaxies. The galaxies are being observed in all polarization products in two different bands, 1.5 GHz (L-band) and 6 GHz (C-band), and over 3 different EVLA array configurations. This is the first comprehensive radio continuum survey of halos to include all polarization products.

Our scientific goals include understanding the physical conditions and origin of gaseous halos, probing cosmic ray transport, and determining outflow speeds and the ultimate fate of the gas. Mapping the halo magnetic field configuration and investigating how fields couple to outflows are particularly important goals, as is examining the FIR-radio continuum relation in halos. We will also measure synchrotron scale heights and attempt to reconcile these with models that focus on high energy (including gamma-ray) emission. Ancillary data, such as infra-red and X-ray data will be applied to some of these questions.

This survey exploits the new capabilities of the EVLA, especially the wide bandwidths that contribute to reducing on-source integration times in the detection of galaxy halos. With up to 405 hours of observing time, our combination of number of galaxies observed, range of spatial scales probed, and low noise levels (see Tables 1 and 2) significantly improve upon previous surveys of edge-on galaxies carried out at these two frequencies; in the case of noise levels, the improvement is more than an order of magnitude. Spectral index variations can also be observed and used to separate thermal from non-thermal emission as well as to model non-thermal spectral index variations in

regions of sufficiently high signal-to-noise.

Our first CHANG-ES test observations of NGC 4631 at C array, along with details as to the data reduction procedures, are reported in Paper II.

JAI and DJS would like to thank the staff at the EVLA for their warm welcome and assistance during their sojourn in Socorro. Research at Ruhr-Universität, Bochum, is supported by Deutsche Forschungsgemeinschaft through grants, FOR1048 and FOR1254. The Digitized Sky Surveys were produced at the Space Telescope Science Institute under U.S. Government grant NAG W-2166. The Second Palomar Observatory Sky Survey (POSS-II) was made by the California Institute of Technology with funds from the National Science Foundation, the National Geographic Society, the Sloan Foundation, the Samuel Oschin Foundation, and the Eastman Kodak Corporation. The National Radio Astronomy Observatory is a facility of the National Science Foundation operated under cooperative agreement by Associated Universities, Inc.

Facilities: EVLA

REFERENCES

- Abdo et al. 2010, ApJ, 709, L152
- Acciari, V. A., et al. 2009, Nature, 462, 770
- Allen, R. J., Baldwin, J. E., & Sancisi, R. 1978, A&A, 62, 397
- Acero, F., et al. 2009, Science 326, 1080
- Azimlu, M., Marciniak, R., & Barmby, P. 2011, AJ, 142, 139
- Baugh, C. M. 2006, Rept. Prog. Phys., 69, 3101
- Beck, R., Brandenburg, A., Moss, D., Shukurov, A., & Sokoloff, D. 1996, ARA&A, 34, 155
- Benjamin, R. A. 2002, Seeing Through the Dust: The Detection of HI and the Exploration of the ISM in Galaxies, ASP Conference Proceedings, San Francisco: Astronomical Society of the Pacific, Eds: A. R. Taylor, T. L. Landecker, and A. G. Willis, Vol. 276, 201
- Boulares, A. & Cox, D. P. 1990, ApJ, 365, 544
- Brar, R. S., Irwin, J. A., & Saikia, D. J. 2003, MNRAS, 340, 269
- Braun, R., Heald, G., & Beck, R. 2010, A&A, 514, 42
- Bregman, J. N., & Houck, J. C. 1997, ApJ, 485, 159
- Bregman, J. N., & Pildis, R. A. 1994, ApJ, 420, 570
- Breitschwerdt, D., McKenzie, J. F., & Völk, H. J. 1991, A&A, 245, 79
- Brentjens, M. A., & de Bruyn, A. G. 2005, A&A, 441, 1217
- Briggs, D. S. 1995, High Fidelity Deconvolution of Moderately Resolved Sources, PhD Thesis, The New Mexico Institute of Mining and Technology, Socorro, NM
- Calzetti, D., et al. 2007, ApJ, 666, 870
- Chakraborti, S., & Ray, A. 2011, ApJ, 728, 24
- Chaves, T., & Irwin, J. A. 2001, ApJ, 557, 646
- Condon, J. J. 1992, ARA&A, 30, 575
- Condon, J. J., et al. 1998, AJ, 115, 1693
- Condon, J. J., Cotton, W. D., & Broderick, J. J. 2002, AJ, 124, 675
- Dahlem, M., Lisenfeld, U., & Golla, G. 1995, ApJ, 444, 119
- Dale, D. A., & Helou, G. 2002, ApJ, 576, 159
- Dumke, M., Krause, M., & Wielebinski, R., & Klein, U. 1995, A&A, 302, 691
- Duric, N., Irwin, J. A., & Bloemen, H. 1998, A&A, 331, 428
- Ekers, R. D., & Sancisi, R. 1977, A&A, 54, 973
- Everett, J. E., Zweibel, E. G., Benjamin, R. A., McCammon, D., Rocks, L., & Gallagher III, J. S. 2008, ApJ, 674, 258
- Everett, J. E., Schiller, Q. G., & Zweibel, E. G. 2010, ApJ, 711, 13
- Ferrarese, L., & Merritt, D. 2000, ApJ, 539, 9

- Fraternali, F., et al. 2002, *ApJ*, 578, 109
- Fraternali, F., Oosterloo, T., & Sancisi, R. 2004, *A&A*, 424, 4
- Fraternali, F., & Binney, J. J. 2006, *MNRAS*, 449, 449
- Fraternali, F., Binney, J. J., Oosterloo, T., & Sancisi, R. 2007, *New A Rev.*, 51, 95
- Gebhardt, K., et al. 2000, *ApJ*, 539, 13
- Gisinger, C., Fromang, S., & Dormy, E. 2009, *MNRAS*, 394, 84
- Hanasz, M., Otmianowska-Mazur, K., & Lesch, H. 2002, *A&A*, 386, 347
- Hanasz, M., Wóltański, D., & Kowalik, K. 2009, *ApJ*, 706, 155
- Heald, G. H., Rand, R. J., Benjamin, R. A., & Bershady, M. A. 2007, *ApJ*, 663, 933
- Heald, G. H., et al. 2009, *A&A*, 503, 409
- Heesen, V., Beck, R., Krause, M., & Dettmar, R.-J. 2009a, *A&A*494, 563
- Heesen, V., Krause, M., Beck, R., & Dettmar, R.-J. 2009b, *A&A*, 506, 1123
- Helou, G., et al. 1985, *ApJ*, 298, L7
- Howk, J. C., & Savage, B. D. 1999, *AJ*, 117, 2077
- Hummel, E., & Dettmar, R.-J. 1990, *A&A*, 236, 33
- Hummel, E., van Gorkom, J. H., & Kotanyi, C. G. 1983, *ApJ*, 267, 5
- Hummel, E., & van der Hulst, J. M. 1989, *A&AS*, 81, 51
- Hummel, E., Beck, R., & Dettmar, R.-J. 1991, *A&AS*, 87, 309
- Ipavich, F. M. 1975, *ApJ*, 196, 107
- Irwin, J. A., English, J., & Sorathia, B. 1999, *AJ*, 117, 2102
- Irwin, J. A., Saikia, D. J., & English, J. 2000, *AJ*, 119, 1592
- Irwin, J. A., & Seaquist, E. R. 1988, *ApJ*, 335, 658
- Irwin, J. A., & Seaquist, R. R. 1990, *ApJ*, 353, 469
- Irwin, J. A. et al. 2011, *MNRAS*, 410, 1423
- Irwin, J. A. et al. 2012, *AJ*, Paper II
- Kennicutt, R. C., Jr. 1998, *ARA&A*, 36, 189
- Kennicutt, R. C., Jr. 2008, in *Infrared Diagnostics of Galaxy Evolution*, ASP Conf. Series, Vol. 381, 103
- Krause, M. 2004, in *The Magnetized Interstellar Medium*, Eds. B. Uyaniker, W. Reich, and R. Wielebinski, Copernicus GmbH, Katlenburg-Lindau., 173
- Krause, M. 2009, in *Magnetic Fields in the Universe II: From Laboratory and Stars to the Primordial Universe*, Revista Mexicana de Astronomía y Astrofísica (Serie de Conferencias), Eds. A. Esquivel, J. Franco, G. Garcia-Segura, E. M. de Gouveia Dal Pino, A. Lazarian, S. Lizano, & A. Raga, Vol. 36, 25
- Krause, M. 2011, in *Proc. of Magnetic Fields in the Universe III: From Laboratory and Stars to Primordial Structures*, Eds. M. Soida, K. Otmianowska-Mazur, E.M. de Gouveia Dal Pino & A. Lazarian, Zakopane, Poland, arXiv:1111.7081
- Kronberg, P. P., Lesch, H. & Hopp, U. 1999, *ApJ*, 511, 56
- Lee, S.-W., Irwin, J. A., Dettmar, R.-J., Cunningham, C. T., Golla, G., & Wang, Q. D. 2001, *A&A*, 377, 759
- Li, Z., et al. 2011, *ApJ*, 730, 84
- Li, J.-T., Wang, Q. D., Li, Z., & Chen, Y. 2011, *ApJ*, 737, 41
- Mao, S. A., et al. 2010, *ApJ*, 714, 1170
- Mac Low, M., & Ferrara, A. 1999, *ApJ*, 513, 142
- Martin, C., & Kern, B. 2001, *ApJ*, 555, 258
- Martos, M., & Cox, D. P. 1998, *ApJ*, 509, 703
- Moskalenko, I. V. & Strong, A. W. 1998, *ApJ*, 493, 694
- Moskalenko, I. V., et al., 2002, *ApJ*, 565, 280

- Moss, D., & Sokoloff, D. 2008, A&A, 487, 197
- Moss, D., Sokoloff, D., Beck, R., & Krause, M. 2010, A&A, 512, 61
- Moustakas, J., & Kennicutt, R. C., Jr. 2006, ApJS, 164,81
- Murphy, E. J., et al. 2006, ApJ, 638, 157
- Murphy, E. J., et al. 2008, ApJ, 678, 828
- Murphy, E. J., et al. 2009, ApJ, 694, 1435
- Norman, C. A. & Ikeuchi, S. 1989, ApJ, 345, 372
- Oosterloo, T., Fraternali, F., & Sancisi, R. 2007, AJ, 134, 1019
- Paturel, G., et al. 2003 A&A, 412, 45
- Pohl, M., & Schlickeiser, R. 1990, A&A, 239, 424
- Porter, T. A., et al., 2008, ApJ, 682, 400
- Rand, R. J. 1996, ApJ, 462, 712
- Rand, R. J., & Stone, J. M. 1996, AJ, 111, 190
AJ, 105, 2098
- Rand, R. J., Wood, K., Benjamin, R. A., & Meidt, S. E. 2011, ApJ, 728, 163
- Rossa, J., & Dettmar, R.-J. 2003, A&A, 406, 493
- Rossa, J., Dahlem, M., Dettmar, R.-J., van der Marel, R. P. 2008, arXiv:0804.3819
- Sanders, D. B., Mazzarella, J. M., Kim, D.-C., Surace, J. A., & Soifer, B. T. 2003, AJ, 126, 1607
- Sanders, D. B., & Mirabel, I. F. 1996, ARA&A, 34, 749
- Satyapal, S., Böker, T., McAlpine, W., Gliozzi, M., Abel, N. P., & Heckman, T. 2009, ApJ, 704, 439
- Schaap, W. E., Sancisi, R., & Swaters, R. A. 2000, A&A, 356, 49
- Shapiro, P. R., & Field, G. B. 1976, ApJ, 205, 762
- Shukurov, A., Sokoloff, D., Subramanian, K., & Brandenburg, A. 2006, A&A, 448, L33
- Silich, S., et al. 2006, A&A, 448, 123
- Soida, M., Krause, M., Dettmar, R.-J., & Urbanik, M. 2011, A&A, 531, 127
- Spekkens, K., Irwin, J. A., & Saikia, D. J. 2004, MNRAS, 352, 1145
- Solanes, J. M., Sanchis, T., Salvador-Solé, E., Giovanelli, R., & Haynes, M. P. 2002, AJ, 124, 2440
- Strickland, D. K., Heckman, T. M., Colbert, E. J. M., Hoopes, C. G., & Weaver, K. A. 2004, ApJ, 606, 829
- Strong, A. W. 1978, A&A, 66, 205
- Strong, A. W., et al. 2000, ApJ, 537, 763
- Strong, A. W., et al., 2004, A&A, 422, L47
- Strong, A. W., et al. 2009, arXiv:0907.0559v1
- Strong, A. W., et al. 2010, ApJ, 722, L58
- Sur, S., Shukurov, A., & Subramanian, K. 2007, MNRAS, 377, 874
- Swaters, R. A., Sancisi, R., & van der Hulst, J. M. 1997, ApJ, 491, 140
- Tabatabaei, F. S., et al. 2007, A&A, 466, 509
- Tabatabaei, F.S., Berkhuijsen, E.M., Beck, R., & Schinnerer, E. 2012, ApJ, submitted
- Tüllmann, R., Dettmar, R.-J., Soida, M., Urbanik, M., & Rossa, J. 2000, A&A, 364, L36
- Tüllmann, R., et al. 2003, A&A, 412, 69
- Tüllmann, R., Breitschwerdt, D., Rossa, J., Pietsch, W., & Dettmar, R.-J. 2006, A&A, 457, 779
- Tully, B. *Nearby Galaxies Catalog*, Cambridge and New York: Cambridge University Press, 1988
- Wang, Q. D. 2010, Pub. of the National Academy of Science, Vol. 107, Iss. 16, p. 7168
- Wang, Q. D., et al. 1995, ApJ, 439, 176
- Wang, Q. D., Immler, S., Walterbos, R., Lauroesch, J. R., & Breitschwerdt, D. 2001, ApJ, 555, L99
- Wakker, B. P., & van Woerden, H. 1997, ARA&A, 35, 217

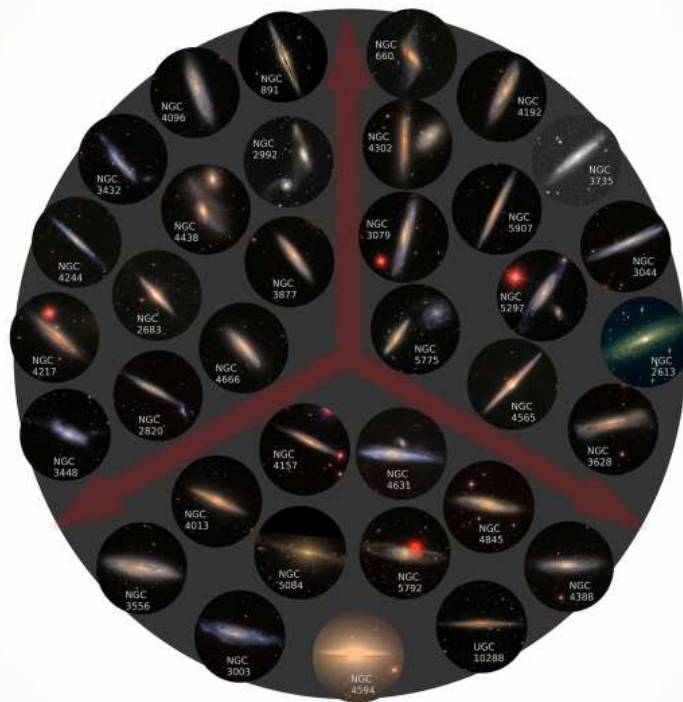
Whaley, C. H., Irwin, J. A., Madden, S. C., Gal-
liano, F., Bendo, G. J. 2009, MNRAS, 395, 97

Wilson, A. S., & Ulvestad, J. S. 1983, ApJ, 275, 8

Zimmer, F., Lesch, H., & Birk, G. T. 1997, A&A,
320, 746

CHANG-ES
Continuum
HALos in
Nearby
Galaxies
- an
EVLA
Survey

EVLA
Karl G. Jansky
(Expanded)
Very
Large
Array



Optical Image credit: SDSS, DSS, CFHT Hawaiian Sky, ESO VIMOS, CTIO AstroDon.

Fig. 1.— The CHANG-ES logo, showing optical images of the galaxy sample and the ‘Y’ shape of the EVLA.

TABLE 1
THE CHANG-ES GALAXY SAMPLE

Name	RA (J2000) ^a (h m s)	DEC (J2000) ^a (d m s)	i^b (deg)	d_{25}^c (')	V_{\odot}^d (km/s)	D^e (Mpc)	Type ^f	Nuclear Type ^a	$S_{1.4}$ (ref) ^g (mJy)	L_{FIR}^h ($10^9 L_{\odot}$)	SFR ⁱ ($M_{\odot} \text{ yr}^{-1}$)	$\log(M_T)^j$ ($\log(M_{\odot})$)	ρ^k (Mpc^{-3})
N 660	01h43m02.40s	+13d38m42.2s	77	7.2	856	12.3	SBa	HII,LINER	373 (A)	16.8	5.7	10.73	0.12
N 891	02h22m33.41s	+42d20m56.9s	84	12.2	529	9.48	Sb	HII	286 (C)	12.1	4.7	11.19	0.55
N 2613	08h33m22.84s	-22d58m25.2s	85	6.8	1679	23.4	Sb	HII	69 (B)	9.68	4.6	11.58	0.15
N 2683	08h52m41.35s	+33d25m18.5s	79	9.1	415	6.27	Sb	LINER,Sy2	84 (B)	0.86	0.36	10.81	0.09
N 2820	09h21m45.58s	+64d15m28.6s	90	4.1	1576	26.5	SBc		46.6 (A)	5.91	2.0	10.87	0.28
N 2992	09h45m42.00s	-14d19m35.0s	90	4.4	2212	34.0	Sa	Sy1,Sy2	226 (A)	16.6	7.2	11.24	0.21
N 3003	09h48m36.05s	+33d25m17.4s	90	6	1480	25.4	Sbc		30.4 (A)	3.87	1.5	10.75	0.64
N 3044	09h53m40.88s	+01d34m46.7s	90	4.4	1335	20.3	SBc	HII	103 (A)	7.14	2.6	10.81	0.19
N 3079	10h01m57.80s	+55d40m47.3s	88	7.7	1125	20.6	SBcd	LINER,Sy2	821 (C)	39.1	13	11.27	0.29
N 3432	10h52m31.13s	+36d37m07.6s	82	4.9	611	9.42	SBm	LINER,HII	120 (B)	1.31	0.39	10.19	0.19
N 3448	10h54m39.24s	+54d18m18.8s	78	4.9	1391	24.5	S0-a		51.3 (A)	6.65	2.1	10.95	0.24
N 3556	11h11m30.97s	+55d40m26.8s	81	7.8	697	14.09	SBc	HII	217 (A)	12.5	4.9	10.78	0.15
N 3628	11h20m17.01s	+13d35m22.9s	87	14.8	846	8.50	Sb	HII,LINER	470 (C)	6.99	2.3	11.17	0.39
N 3735	11h35m57.30s	+70d32m08.1s	85	4	2696	42.0	Sc	Sy2	85.8 (A)	24.3	11	11.38	0.19
N 3877	11h46m07.80s	+47d29m41.2s	85	5.1	894	17.7	Sc	HII	40.7 (A)	5.19	2.2	10.74	1.53
N 4013	11h58m31.38s	+43d56m47.7s	84	4.7	835	16.0	Sb	HII,LINER	38.2 (A)	4.25	1.8	10.79	1.34
N 4096	12h06m01.13s	+47d28m42.4s	82	6.4	577	10.32	SABc	HII	51.4 (A)	1.77	0.75	10.59	0.40
N 4157	12h11m04.37s	+50d29m04.8s	90	7	771	15.6	SABb	HII	185 (A)	9.18	3.8	11.00	1.19
N 4192	12h13m48.29s	+14d54m01.2s	83	8.7	-142	13.55 (V)	SABb	HII,Sy,LINER	23.0 (A)	3.3	1.49	11.15	1.44
N 4217	12h15m50.90s	+47d05m30.4s	78	5.1	1028	20.6	Sb	HII	120 (A)	11.8	5.3	11.03	0.95
N 4244	12h17m29.66s	+37d48m25.6s	90	15.8	247	3.30	Sc	HII	20.3 (C)	<0.03	< 0.01	10.02	0.39
N 4302	12h21m42.48s	+14d35m53.9s	89	4.7	1118	19.41 (V)	Sc	Sy,LINER	34.8 (A)	5.08	2.3	10.90	3.60
N 4388	12h25m46.75s	+12d39m43.5s	79	5.6	2607	16.60 (V)	Sb	Sy2	119 (A)	4.71	2.6	10.94	1.56
N 4438	12h27m45.59s	+13d00m31.8s	78	9.1	259	10.39 (V)	Sa	LINER	63.3 (A)	0.90	0.32	10.91	2.67
N 4565	12h36m20.78s	+25d59m15.6s	90	16.2	1228	27.1	Sbc	Sy3,Sy1.9	134 (D)	15.7	7.9	11.80	1.00
N 4594	12h39m59.43s	-11d37m23.0s	79	8.4	1127	12.7	Sa	LINER,Sy1.9	93.4 (A)	1.59	0.68	11.08	0.32
N 4631	12h42m08.01s	+32d32m29.4s	85	14.7	613	7.55	SBcd		772 (C)	8.49	2.9	10.74	0.41
N 4666	12h45m08.59s	-00d27m42.8s	76	4.2	1516	27.5	SABc	HII,LINER	434 (A)	53.8	20	11.13	0.54
N 4845	12h58m01.19s	+01d34m33.0s	81	4.8	1228	16.98 (V)	Sab	HII,LINER	43.3 (A)	5.17	1.8	11.32	0.49
N 5084	13h20m16.92s	-21d49m39.3s	90	12.5	1728	23.4	S0	poss.LINER	45.9 (A)	0.49	< 0.21	11.91	0.29
N 5297	13h46m23.68s	+43d52m20.5s	89	5.3	2404	40.4	SABc		23.0 (A)	8.09	3.9	11.28	0.79
N 5775	14h53m58.00s	+03d32m40.1s	84	3.9	1582	28.9	Sbc		280 (A)	38.1	14	11.09	0.67
N 5792	14h58m22.71s	-01d05m27.9s	81	7.2	1930	31.7	SBb	HII	51.8 (A)	17.2	6.4	11.47	0.52
N 5907	15h15m53.77s	+56d19m43.6s	90	11.2	666	15.26	Sc	HII	50.5 (A)	5.56	2.7	11.32	0.26
U10288	16h14m24.80s	-00d12m27.1s	90	4.9	2046	34.1	Sc		26.1 (A)	2.55	1.3	11.07	0.23

NOTE.—Data are from Tully (1988) unless otherwise indicated.

^aFrom the NASA Extragalactic Database (NED).

^bInclination, $i = 3deg + \cos^{-1}(\sqrt{((b/a)^2 - 0.2^2)/(1 - 0.2^2)})$, where b/a is the minor to major axis ratio.

^cObserved blue diameter at the 25th mag/arcsec² isophote.

^dHeliocentric radial velocity.

^eDistance from NED, assuming $H_0 = 73 \text{ km s}^{-1} \text{ Mpc}^{-1}$ and correcting for Virgo Cluster and Great Attractor perturbations, except for Virgo Cluster galaxies which have been taken from (Solanes et al. 2002); the latter are indicated by (V).

^fFrom HYPERLEDA, <http://leda.univ-lyon1.fr/>, see also Paturel et al. (2003).

^gFlux density at 1.4 GHz from refs: (A) NRAO VLA Sky Survey (NVSS Condon et al. 1998), (B) Irwin, English & Sorathia (1999), (C) Strong et al. (2004), (D) Condon et al. (2002).

^hFIR luminosity from $L_{FIR} = 4\pi D^2 F_{FIR}$, where $F_{FIR} = 1.26 \times 10^{-14} (2.58 S_{60} + S_{100}) \text{ W m}^{-2}$ for S in Jy (see Sanders & Mirabel 1996), representing the flux in the 40.2 to 122.5 μm range. We take S from Sanders et al. (2003) or, if not available, from the most recent entry in NED, usually the IRAS Faint Source Catalog (FSC). N 4302 had no NED entry and was taken from the FSC directly.

ⁱ $\text{SFR}(\text{M}_{\odot} \text{ yr}^{-1}) = 4.5 \times 10^{-44} L_{TIR}(\text{ergs s}^{-1})$ (Kennicutt 1998) where L_{TIR} (3 to 1100 μm) is computed from S_{25} , S_{60} and S_{100} according to the prescription in Dale & Helou (2002) and the flux densities are from the same sources as in the previous note. These values may be refined in the future with improved IR data (see, e.g. Murphy et al. 2008).

^j(Log of) the total mass in units of M_{\odot} , where $M_T = W^2 d / (8G)$. W is the HI line width corrected for random gas motions and galaxy inclination, and d is the galaxy's linear diameter calculated from d_{25} and the galaxy's distance, corrected for the effects of projection and obscuration (values adjusted to our distance).

^kDensity of galaxies brighter than -16 mag in the vicinity of the galaxy. The local density was determined on a 3D-grid at 0.5 Mpc spacing. No correction has been made for the fact that our distances differ somewhat from those of Tully (1988).

TABLE 2
ESTIMATED OBSERVING TIME, RMS & SPATIAL COVERAGE FOR CHANG-ES

Array: ν_0^a	Time/pt. ^b	Theor. rms ^c ($\mu\text{Jy beam}^{-1}$)	Confusion ^d ($\mu\text{Jy beam}^{-1}$)	θ_{HPBW}^e (arcsec)	Lin. Res. ^f Min/max (pc/kpc)	θ_{LAS}^g (arcmin)
B: 1.5 GHz	2 hrs	7.7	–	4.3	69/0.88	2.0
C: 1.5 GHz	30 min	16	9	14	224/2.85	16.2
6 GHz	3 hrs	2.4	0.2	3.5	56/0.71	4.0
D: 1.5 GHz	20 min	20	89	46	736/9.4	16.2
6 GHz	40 min	4.8	2.3	12	192/2.4	4.0

NOTE.—These estimates represent a best-case scenario in which there is no RFI or other errors.

^aEVLA array configuration and central frequency.

^bOn-source time per pointing, not including overheads. At 6 GHz, the field of view is smaller and the larger galaxies require more than one pointing.

^cTheoretical noise, ignoring confusion, for each polarization product. Robust weighting (Briggs 1995) is assumed. At 6 GHz, the bandwidth, $B = 2$ GHz and at 1.5 GHz, $B = 500$ MHz. See the EVLA Observational Status Summary (OSS) at <http://evlaguides.nrao.edu/index.php?title=Category:Status>.

^dEstimated confusion limits (from the OSS). These confusion limits should only apply to total intensity, I, but not to polarization products, Q, U or V.

^eSpatial resolution, assuming uniform weighting. Actual values will be larger when robust weighting is used. Given the wide frequency bands and possibility of a variety of uv weightings, the range of spatial resolution is actually greater than noted here.

^fMinimum and maximum linear resolution for minimum and maximum galaxy distances, respectively, corresponding to the spatial resolutions of the previous column.

^gLargest angular size scale detectable by the array.